

# Prediction of Icing Effects on the Lateral/Directional Stability and Control of Light Airplanes

Amanda Lampton\* and John Valasek†  
Texas A&M University, College Station, TX 77843-3141

## Abstract

The accumulation of ice on an airplane in flight is one of the leading contributing factors to general aviation accidents, and to date only relatively sophisticated methods based on detailed empirical data and flight data exist for its analysis. This paper develops a methodology and simulation tool for a preliminary yet accurate evaluation of airplane dynamical response and stability and control characteristics due to icing. It uses only basic mass properties, configuration, and propulsion data, together with known icing data obtained for similar configurations. Existing icing data for a light airplane is suitably modified and applied to a non real-time, six degree-of-freedom simulation model of a different but similar light airplane, developed from empirical data and Data Compendium methods. The component build-up method is used to implement icing effects on the wing alone, horizontal tail alone, and various unequal distributions of combined wing and horizontal tail icing as well as ice accretion on only one half of the wing. Results presented in the paper are limited to the roll axis and yaw axis maneuvers with various levels and distributions of ice accretion show that the methodology captures the basic detrimental effects of ice accretion on roll and yaw response and lateral stability, in addition to the sensitivity of pilot control response.

## Nomenclature

$A$	= Plant matrix
$B$	= Control distribution matrix
$C$	= Output matrix
$C_{(A)}$	= Arbitrary stability and control derivative
$C_{(A)_{\text{tot}}}$	= Arbitrary stability and control derivative with icing effects
$C_D$	= Airplane drag coefficient
$C_L$	= Airplane lift coefficient
$C_l$	= Airplane rolling moment coefficient
$C_m$	= Airplane pitching moment coefficient
$C_n$	= Airplane yawing moment coefficient
$C_Y$	= Airplane sideforce coefficient
$C_Z$	= Stability Z-axis coefficient
$\bar{c}$	= Mean geometric chord

---

\*Graduate Research Assistant, Flight Simulation Laboratory, Aerospace Engineering Department.  
Student Member AIAA. [alampton@tamu.edu](mailto:alampton@tamu.edu)

†Associate Professor and Director, Flight Simulation Laboratory, Aerospace Engineering Department.  
Associate Fellow AIAA. [valasek@tamu.edu](mailto:valasek@tamu.edu)

$D$	= Carry through matrix
$d$	= Distance along body X-axis
$f_{ice}$	= Icing factor
$g$	= Gravitational acceleration
$h$	= Integration step size
$I_{xx}$	= Airplane moment of inertia about X-axis
$I_{xz}$	= Airplane moment of inertia about XZ-plane
$I_{zz}$	= Airplane moment of inertia about Z-axis
$i$	= Index, imaginary component
$j$	= Imaginary component
$kts$	= knots
$k'_{c_a}$	= Coefficient icing factor constant
$L$	= Roll angular acceleration
LTI	= Linear time invariant
LWC	= Liquid Water Content
$M$	= Pitch angular acceleration; modal matrix
MVD	= Median Volumetric Diameter
$N$	= Yaw angular acceleration
$nframes$	= Number of time steps
$P$	= Aircraft body-axis roll rate
$p$	= Perturbed aircraft body-axis roll rate
$pla$	= Powel lever angle
$\bar{q}$	= Dynamic pressure
$R$	= Aircraft body-axis yaw rate
$r$	= Perturbed aircraft body-axis yaw rate
$rad$	= Radian
$S$	= Wing area
$sec$	= Second
$t$	= Time
$U$	= Control input vector
$V$	= Aircraft velocity in the body-axis y-direction
$W$	= Aircraft velocity in the body-axis z-direction
$\dot{w}$	= Incremental change in the stability axis aircraft velocity in the z-direction
$X$	= Linear acceleration in the body x-axis direction
$\mathbf{X}$	= State vector
$\dot{\mathbf{X}}$	= Derivative of state vector
$Y$	= Linear acceleration in the body y-axis direction
$\mathbf{Y}$	= Output vector
$Z$	= Linear acceleration in the body z-axis direction

*Greek*

$\alpha$	= Angle-of-attack
$\dot{\alpha}$	= Incremental change in angle-of-attack
$\beta$	= Sideslip angle
$\dot{\beta}$	= Incremental change in sideslip angle
$\Gamma$	= Discrete control distribution matrix
$\delta$	= Control deflection angle
$\zeta$	= Damping ratio

$\eta_{ice}$	= Icing severity parameter
$\Theta_1$	= Aircraft steady-state pitch attitude angle
$\theta$	= Pitch attitude angle
$\dot{\theta}$	= Incremental change in pitch attitude angle
$\xi$	= Modal vector
$\tau$	= Time constant; dummy time variable
$v$	= Eigenvector
$\Phi$	= Aircraft roll attitude angle; discrete plant matrix
$\phi$	= Roll attitude angle
$\dot{\phi}$	= Incremental change in roll attitude angle
$\Psi_1$	= Aircraft steady-state heading angle
$\psi$	= Heading angle
$\dot{\psi}$	= Incremental change in heading angle
$\omega$	= Frequency

### *Subscripts*

0	= Derivative with respect to zero angle-of-attack; initial condition
1	= Steady-state; first mode
2	= Second mode
a	= Aileron
d	= Dutch roll mode
ice	= Ice accretion effect
iced	= Ice accretion effect
k	= Index for discretized model
m	= Modal
mgc	= Mean geometric chord
$p$	= Derivative with respect to aircraft roll rate
r	= Rudder; Roll mode
$r$	= Derivative with respect to aircraft yaw rate
s	= Spiral mode
$u$	= Derivative with respect to stability x-axis aircraft velocity
$\beta$	= Derivative with respect to sideslip angle
$\delta_a$	= Derivative with respect to aileron deflection angle
$\delta_r$	= Derivative with respect to rudder deflection angle

### *Superscripts*

$T$	= Transpose
-----	-------------

## I. Introduction

Inclement weather accounted for an average of 19.6% of environment related reported general aviation accidents annually from 1998 to 2000 according to the National Transportation Safety Board (NTSB).<sup>1,2,3</sup> Of this annual percentage, icing conditions accounted for 2.9% of general aviation accidents in 1997, 2.4% in 1998, 3.6% in 1999, and 2.7% in 2000, where 36.4%, 55.6%, 46.2%, and 40.0% of those resulted in fatalities in 1997, 1998, 1999, and 2000, respectively.<sup>1,2,3,4</sup> Rime, glaze, and mixed ice along the leading edge of lifting surfaces all have detrimental effects on aircraft performance. Although anti-icing devices such as de-icing boots and heating strips help, ice accretions can still build up and affect the aircraft adversely by decreasing static lateral stability, especially in the case when the aircraft does not

develop ice accretions evenly between wing halves. Additionally, malfunctions of these anti-icing systems can result in ice buildup aft of the devices themselves, or ice buildup between the cycles of the de-icing systems. The type and severity of ice accretions is highly dependent on a number of factors. These include, but are not limited to, the following: velocity of the aircraft, exposure time, atmospheric air temperature, Liquid Water Content (LWC), and Median Volumetric Diameter (MVD).

The danger of a lateral maneuver with ice accretions on the aircraft lays in the susceptibility of the ice causing a separation bubble (Figure 1).<sup>5</sup> This phenomenon is usually caused by a horn of ice disrupting the flow of air over the airfoil and creating an adverse pressure gradient. This disruption forms a separation bubble that reattaches further downstream. However, increasing the aileron deflection angle increases the relative angle-of-attack over the wing as the aircraft rolling moment increases, thus pushing the reattachment point farther downstream and increasing the size of the separation bubble.<sup>6</sup> As the bubble increases in size, aileron effectiveness decreases and full departure of the aircraft becomes more likely. Ice accretions on the vertical tail can form a similar separation bubble phenomena. The effect of full tail icing has been shown to decrease weathercock stability,  $C_{n_p}$ , as well as reduce rudder effectiveness.<sup>7</sup> Bragg *et al.* have developed an icing effects model applicable to any performance, stability, or control derivative affected by icing.<sup>8</sup> The model is characterized by dependence on

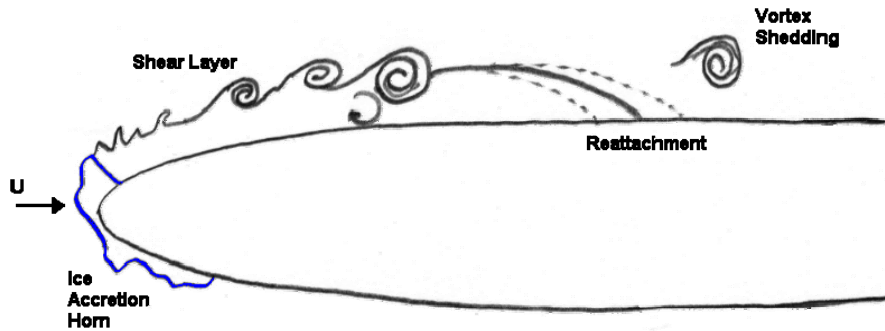


Figure 1. Schematic of Upper Surface Separation Bubble Aft of Leading-Edge Ice Accretion<sup>5</sup>

atmospheric conditions, susceptibility of an aircraft to icing, and a given derivative as seen in Eq. 1.

$$C_{(A)_{iced}} = (1 + \eta_{ice} k'_{C_A}) C_{(A)} \quad (1)$$

This model is currently in the early stages of development with many of the influencing factors still unknown.<sup>8</sup> The model was then integrated into a Flight Dynamics and Control toolbox for MATLAB and Simulink<sup>9</sup>, which produces results showing the possible changes of an aircraft's stability derivatives over time with icing effects.

The practicality of using an autopilot during icing conditions has also been studied. Sharma *et al.* has designed a pitch angle hold autopilot that considers ice accretion severity when processing the commanded pitch attitude angle; the goal being to maintain the stability of the aircraft.<sup>10</sup> The commanded value for the pitch attitude angle is then modified based on an envelope protection algorithm that references flight test data of ice severity and wing stall angle-of-attack.<sup>10</sup> The purpose being not to allow the aircraft to reach the icing modified wing stall angle-of-attack.<sup>10</sup> Currently, the autopilot is tailored specifically for the DeHavilland Twin Otter.<sup>10</sup> The algorithms could certainly be modified for another aircraft, but the development of a new linear and nonlinear model of the aircraft in question is required, the gain scheduling would have to be tailored to the aircraft, and the flight test data on which the envelope protection scheme is based would have to be recorded for the aircraft in question.

The area of forensic engineering is also concerned with the effect ice has on climb performance and aerodynamic degradation.<sup>11</sup> The research described in Ref. 11 concerns the dangerous reduction in stall angle-of-attack and how climbing at high angles-of-attack could approach this reduced stall angle causing an unexpected wing stall. The nonlinear simulation incorporating the effects of ice accretion was set up specifically for a jet trainer in an attempt to project the trajectory of a crash caused by ice accretion.<sup>11</sup>

Much other research in the area of the influence of ice regards airfoil aerodynamics. Lee and Bragg explore the changes in airfoil section lift, drag, and pitching moment with simulated ice shapes.<sup>12</sup> Intercycle ice accretions have a distinct effect on airfoil properties as described in Ref. 13. In this case the buildup of ice between pneumatic boot inflation and the possible ice ridge left just behind where the boot meets the skin of the airfoil is analyzed.<sup>13</sup> The resulting increase in drag, decrease in lift, and change in pitching moment is tabulated.<sup>13</sup> In general, the consensus appears to be that the aerodynamics of an airfoil is degraded by ice accretion such that lift decreases, drag increases, stall angle-of-attack is reduced, and pitching moment is degraded.<sup>11,12,13,14,15</sup>

The contribution of this paper is an alternative and simplified method for the prediction of icing effects on the dynamic response and performance of light airplanes. The approach developed here uses known icing data for a given airplane configuration (obtained from either flight data or wind tunnel data or both) and applies it via appropriate scaling and modification to a different airplane of similar configuration. These icing effects are used in a component buildup fashion to develop a linear time invariant (LTI), six degree-of-freedom, non real-time flight simulation code used for investigating dynamic response, stability, and rolloff tendencies for various levels of ice accretion, and unequal icing distributions between the right and left half of the wing, which can result when flying in icing conditions with a crosswind. The utility of this approach is the ability to investigate the dynamic response due to various icing distributions for airplanes for which icing data does not exist. An additional advantage of this approach compared to earlier work in the literature is the ability to evaluate a variety of time-varying pilot inputs, such as singlets, doublets, and ramps. Because of this feature, the important effect of under-commanding or over-commanding an iced airplane during lateral maneuvers can be evaluated. In total, the approach developed in this paper permits a rapid, first cut analysis of icing effects using only basic, relatively easy to obtain or generate data as a prelude to a highly detailed analysis using sophisticated methods. The scope of this paper is limited to the roll axis and yaw axis, where the most detrimental icing effects are typically experienced.

The paper is organized as follows. First a non-parametric linear model of a Cessna 208B Super Cargomaster (Figure 2) is developed, in which stability and control derivatives are calculated using the DATCOM and *Advanced Aircraft Analysis* (AAA) computer program.<sup>16</sup> Verification of the is accomplished by comparing simulation data to published data.

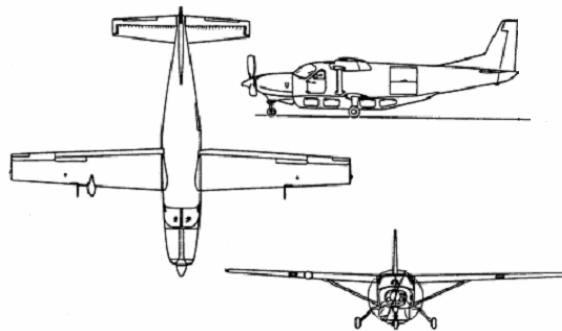


Figure 2. Cessna 208B Super Cargomaster External Characteristics

To ensure the fidelity of the model a modal analysis to examine the characteristics of the flight modes was conducted. In addition, a controllability analysis was conducted to check that the system was indeed linearly independent and controllable. Next, the stability derivatives calculated for each flight condition of interest are used to construct multiple linear time-invariant state-space models used for non real-time simulation. Various levels of ice accretion severity are then added to the clean aircraft simulation based on icing data gathered by NASA Glenn on the DeHavilland Twin Otter.<sup>8</sup> Finally, numerical examples consisting of either a rudder 3-1-2 followed by an aileron doublet or uneven icing between wing halves with different amounts of ice accretion applied to the aircraft are presented. Finally, a summary and conclusions are presented.

## II. State-Space Model Representation

To determine the response of a linear-time-invariant (LTI) system to an arbitrary input signal, it is transformed into a state-space representation of the system. The system analyzed in this paper is a continuous dynamic linear system in the stability axis. Figure 3 shows the body-axis systems for reference.

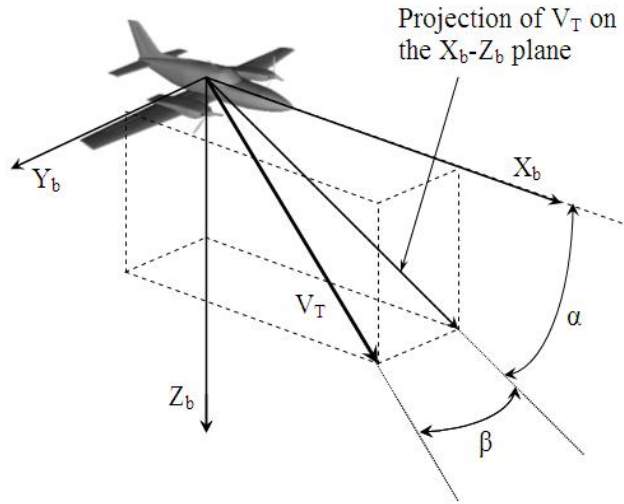


Figure 3. Body Axis System and Aerodynamic Angles

Time-invariance of the model is assumed since the parameters in the model do not change quickly for the relatively slow maneuvers examined here. Consider first the linear time-invariant state-space model of perturbations about the steady-state or trim condition

$$\begin{aligned}\dot{\mathbf{X}} &= \mathbf{A}\mathbf{X} + \mathbf{B}\mathbf{U} \\ \mathbf{Y} &= \mathbf{C}\mathbf{X} + \mathbf{D}\mathbf{U}\end{aligned}\quad (2)$$

where  $\mathbf{X} \in \mathbb{R}^{n \times 1}$  is a state vector,  $\mathbf{A} \in \mathbb{R}^{n \times n}$  is a plant matrix,  $\mathbf{U} \in \mathbb{R}^{m \times 1}$  is an input vector,  $\mathbf{B} \in \mathbb{R}^{n \times m}$  is a control distribution matrix,  $\mathbf{Y} \in \mathbb{R}^{r \times 1}$  is an output vector, and  $\mathbf{C} \in \mathbb{R}^{r \times n}$  and  $\mathbf{D} \in \mathbb{R}^{r \times m}$  are matrices that determine the elements of the output vector.

### A. Lateral/Directional State-Space Model

Following a similar derivation as above, consider the lateral/directional linear equations of motion of this coupled system in stability-axes are defined as Taylor series expansions:

$$\begin{aligned}
\dot{p} &= L_\beta \beta + L_p p + L_r r + L_{\delta_A} \delta_A + L_{\delta_R} \delta_R + \frac{I_{xz}}{I_{xx}} \dot{r} \\
\dot{\phi} &= p + r \tan \Theta_1 \\
\dot{\beta} &= (Y_p p + g \phi \cos \Theta_1 + Y_\beta \beta + (Y_r - U_1) r + Y_{\delta_A} \delta_A + Y_{\delta_R} \delta_R) / U_1 \\
\dot{r} &= N_\beta \beta + N_p p + N_r r + N_{\delta_A} \delta_A + N_{\delta_R} \delta_R + \frac{I_{xz}}{I_{zz}} \dot{p} \\
\dot{\psi} &= r \sec \Theta_1
\end{aligned} \tag{3}$$

These affine in the control, coupled equations assume steady level 1-g trimmed flight in the stability axis system such that  $P_1 = Q_1 = R_1 = V_1 = W_1 = \Phi_1 = 0$ , and  $\Theta_1 = \text{constant}$ . These equations can be decoupled by pre-multiplying by the mass matrix E:

$$E = \begin{bmatrix} 1 & 0 & 0 & -\frac{I_{xz}}{I_{xx}} & 0 \\ 0 & 1 & 0 & 0 & 0 \\ 0 & 0 & 1 & 0 & 0 \\ -\frac{I_{xz}}{I_{zz}} & 0 & 0 & 1 & 0 \\ 0 & 0 & 0 & 0 & 1 \end{bmatrix} \tag{4}$$

Continuing with Eq. 5, the plant matrix is transformed into the lateral/directional decoupled form

$$E^{-1}A = \begin{bmatrix} L'_p & 0 & L'_\beta & L'_r & 0 \\ 1 & 0 & 0 & \tan \Theta_1 & 0 \\ \frac{Y_p}{U_1} & \frac{g \cos \Theta_1}{U_1} & \frac{Y_\beta}{U_1} & \left( \frac{Y_r}{U_1} - 1 \right) & 0 \\ N'_p & 0 & N'_\beta & N'_r & 0 \\ 0 & 0 & 0 & \sec \Theta_1 & 0 \end{bmatrix} \tag{5}$$

in which the primed quantities result from collecting the  $\dot{p}$  and  $\dot{r}$  in the roll rate and yaw rate equations, respectively, and eliminating them from the other equations. The corresponding control distribution matrix with collected terms is

$$E^{-1}B = \begin{bmatrix} L'_{\delta_A} & L'_{\delta_R} \\ 0 & 0 \\ \frac{Y_{\delta_A}}{U_1} & \frac{Y_{\delta_R}}{U_1} \\ N'_{\delta_A} & N'_{\delta_R} \\ 0 & 0 \end{bmatrix} \tag{6}$$

The lateral/directional state and control vectors are represented by

$$\mathbf{X} = [p \quad \phi \quad \beta \quad r \quad \psi]^T \quad (7)$$

$$\mathbf{U} = \begin{bmatrix} \delta_A \\ \delta_R \end{bmatrix} \quad (8)$$

Assembling Eq. 5 – Eq. 8 results in the following state-space model

$$\begin{bmatrix} \dot{p} \\ \dot{\phi} \\ \dot{\beta} \\ \dot{r} \\ \dot{\psi} \end{bmatrix} = \begin{bmatrix} L'_p & 0 & L'_\beta & L'_r & 0 \\ 1 & 0 & 0 & \tan \Theta_1 & 0 \\ \frac{Y'_p}{U_1} & \frac{g \cos \Theta_1}{U_1} & \frac{Y'_\beta}{U_1} & \left( \frac{Y'_r}{U_1} - 1 \right) & 0 \\ N'_p & 0 & N'_\beta & N'_r & 0 \\ 0 & 0 & 0 & \sec \Theta_1 & 0 \end{bmatrix} \begin{bmatrix} p \\ \phi \\ \beta \\ r \\ \psi \end{bmatrix} + \begin{bmatrix} L'_{\delta_A} & L'_{\delta_R} \\ 0 & 0 \\ \frac{Y'_{\delta_A}}{U_1} & \frac{Y'_{\delta_R}}{U_1} \\ N'_{\delta_A} & N'_{\delta_R} \\ 0 & 0 \end{bmatrix} \begin{bmatrix} \delta_A \\ \delta_R \end{bmatrix} \quad (9)$$

Consistent with the scope of this work, which is to determine degradation due to ice accretions for several parameters via numerical simulation, the continuous-time LTI model developed above must be discretized. This discrete-time LTI system is defined as

$$\begin{aligned} \mathbf{X}_{k+1} &= \Phi \mathbf{X}_k + \Gamma \mathbf{U}_k \\ \mathbf{Y}_k &= \mathbf{C} \mathbf{X}_k + \mathbf{D} \mathbf{U}_k \end{aligned} \quad (10)$$

where  $\Phi \in \mathbb{R}^{n \times n}$  and  $\Gamma \in \mathbb{R}^{n \times m}$  are the state transition matrix and discrete control distribution matrix, respectively, and are dependent on  $A \in \mathbb{R}^{n \times n}$ ,  $B \in \mathbb{R}^{n \times m}$ , and  $h$ , the time step of the discrete-time model.  $\Phi$  and  $\Gamma$  of the discrete model are related to their continuous model counterparts,  $A$  and  $B$ , by the following equations:

$$\Phi = e^{Ah} \quad (11)$$

$$\Gamma = \left( \int_0^h e^{A\tau} d\tau \right) B \quad (12)$$

## B. Stability and Control Derivatives

The elements of Eq. 5 and Eq. 6 are determined from non-dimensional stability and control derivatives extracted from AAA for a DATCOM model of the Cessna 208B developed using the Maintenance Manual<sup>17</sup> for the aircraft and verified by flight test data from Ref. 18. AAA is a code based on the USAF Data Compendium (DATCOM). Major assumptions made in the development of the DATCOM model were i) the exact location of the transition point from laminar to turbulent flow on the lifting surfaces, ii) the drag increment due to gaps between lifting and control surfaces, iii) steady flow, and iv) linear model is accurate up to angular displacements of 15° and velocity perturbations up to 100 ft/sec. A universal location of 14% of the chord of the lifting surface is used as the transition point from

laminar to turbulent flow. For the drag increment a value of 0.00036 is used. Values of the stability and control derivatives used for calculations in this paper are provided in Appendix A.

### C. Lateral/Directional Dynamic Characteristics

This section evaluates the lateral/directional dynamical characteristics using the lateral/directional state-space model. The analysis indicates the presence of the three standard modes, Dutch roll, roll, and spiral. All modes are seen to be stable.

$$\text{Dutch Roll Mode:} \quad \lambda_{1,2} = -1.49 \pm 2.54j \quad (13)$$

$$\omega_d = 1.76 \text{ rad/sec}$$

$$\text{Roll Mode:} \quad \zeta_r = 0.484 \quad (14)$$

$$\tau_r = 0.21 \text{ sec}$$

$$\text{Spiral Mode:} \quad \lambda_2 = -0.016 \quad (15)$$

$$\tau_s = 63.68 \text{ sec}$$

### D. Lateral/Directional Modal Analysis

Modal analysis is useful for indicating contributions of each state, and in particular each control, to the various longitudinal modes. The state-space system is converted to modal coordinates using the similarity transformation

$$\mathbf{X} = M\xi \quad (16)$$

where  $\mathbf{X}$  is the state vector,  $M$  is the modal matrix composed of eigenvectors  $M = [v_1 \ v_1 \ \dots \ v_n]$ , and  $\xi$  is the modal vector composed of the modal coordinates  $\xi = [\xi_1 \ \xi_2 \ \dots \ \xi_n]^T$ . Using the derivative of the similarity transformation

$$\dot{\mathbf{X}} = M\dot{\xi} \quad (17)$$

and substituting into Eq. 2 results in

$$\begin{aligned} M\dot{\xi} &= AM\xi + BU \\ Y &= CM\xi + DU \end{aligned} \quad (18)$$

Solving for  $\dot{\xi}$ , the complex modal state-space equations result:

$$\begin{aligned} \dot{\xi} &= M^{-1}AM\xi + M^{-1}BU \\ Y &= CM\xi + DU \end{aligned} \quad (19)$$

with  $A_m = M^{-1}AM$ ,  $B_m = M^{-1}B$ , and  $C_m = CM$ . Note that  $M^{-1}$  will exist if the eigenvalues are distinct. The diagonalized modal matrix  $A_m$  is composed of complex eigenvalues on the diagonal, such that

$$A_m = \begin{bmatrix} \sigma_1 + j\omega_1 & 0 & 0 & \dots & 0 \\ 0 & \sigma_1 - j\omega_1 & & & \dots & 0 \\ \vdots & & & \sigma_2 + j\omega_2 & & \\ 0 & 0 \dots & & & & \sigma_n + j\omega_n \end{bmatrix} \quad (20)$$

For distinct eigenvalues, a real modal state representation is more useful and can be obtained from a block diagonal transformation that maps the complex diagonalized modal matrix  $A_m$  into a real diagonalized modal matrix to produce the form

$$A_m = \begin{bmatrix} \sigma + j\omega & \\ & \sigma - j\omega \end{bmatrix} \rightarrow \begin{bmatrix} \sigma & \omega \\ -\omega & \sigma \end{bmatrix} \quad (21)$$

where each element is either the real or imaginary component of an eigenvalue. Using the values of the stability and control derivatives for the flight condition considered, the resultant real modal matrices are:

$$A_m = \begin{bmatrix} 0 & 0 & 0 & 0 & 0 \\ 0 & -4.839 & 0 & 0 & 0 \\ 0 & 0 & -0.372 & 1.719 & 0 \\ 0 & 0 & -1.719 & -0.372 & 0 \\ 0 & 0 & 0 & 0 & -0.016 \end{bmatrix} \quad (22)$$

$$B_m = \begin{bmatrix} 30.918 & -21.642 \\ 20.608 & 1.910 \\ -1.262 & -4.873 \\ -0.441 & 0.777 \\ -31.427 & 21.619 \end{bmatrix} \quad (23)$$

$$C_m = \begin{bmatrix} 0 & 0.008 & 0.044 & 0.366 & -0.002 \\ 0 & 0.489 & -0.149 & -0.519 & 0.001 \\ 0 & 0.021 & 0.602 & 0 & -0.008 \\ 0 & -0.101 & -0.272 & 0.137 & -0.057 \\ 0.500 & -0.004 & -0.072 & -0.335 & 0.497 \end{bmatrix} \quad (24)$$

The  $A_m$  matrix provides the eigenvalues, number of modes, and orders of the modes. The matrix indicates that there are three modes as stated earlier. From this  $B_m$  for the lateral/directional flight test, it can be determined that the sideslip angle and the aircraft heading is most affected by the ailerons and rudder, whereas the roll rate is only significantly affected by the ailerons. Yaw rate is affected to a lesser extent by the rudder. The inverse modal matrix for the lateral/directional dynamics is

$$\xi = M^{-1}X \quad (25)$$

For the flight condition considered, this results in

$$M^{-1} = \begin{bmatrix} 0 & 1.509 & 4.166 & 8.120 & 1.000 \\ 1.414 & 0.986 & 0.122 & -0.041 & 0 \\ -0.038 - 1.345i & -0.055 + 0.022i & 0.773 + 0.115i & -0.105 + 0.026i & 0 \\ -0.038 + 1.345i & -0.055 - 0.022i & 0.773 - 0.115i & -0.105 - 0.026i & 0 \\ 0.913 & -1.533 & -4.158 & -8.208 & 0 \end{bmatrix} \quad (26)$$

It is seen that the second-order mode (Dutch roll) is made up primarily of yaw rate and to a lesser extent, roll attitude angle. One of the first order modes, as indicated in the second row of Eq. 26, is composed of sideslip and roll rate, while the other first order mode, as indicated in the fifth row of Eq. 26, is composed mainly roll attitude angle and yaw rate. Like the longitudinal modal analysis, these modes and their compositions are to be expected.

### E. Lateral/Directional Controllability

In this case controllability must be checked for both the aileron and rudder. The controllability matrix for each lateral/directional control in the open-loop system is

$$C = [B \quad AB \quad AAB \quad AAAB \quad AAAAB] \quad (27)$$

which has a rank of five for each,  $rank(C) = 5$ , and is non-singular,  $\det(C) \neq 0$ . This result indicates that the lateral/directional system is linearly independent, and therefore controllable.

## III. Simulation Development

The simulation is developed by taking the continuous state-space model and discretizing it using Eq. 12 and Eq. 13. to determine the discrete matrices  $\Phi$  and  $\Gamma$ . The initial state vector is also set. Note that the state, control, and output vectors for the continuous model as stated in earlier sections are represented by  $\mathbf{X}$ ,  $\mathbf{U}$ , and  $\mathbf{Y}$ , respectively. Since the rest of the simulation development is a discrete model dependent on perturbations of the states and controls around the steady-state condition, the state, control, and output vectors are represented by  $\mathbf{x}$ ,  $\mathbf{u}$ , and  $\mathbf{y}$ , respectively, so that the two types of models can be easily distinguished. Thus, since the simulation begins with steady level flight, the initial perturbation state-vector is represented by

$$\mathbf{x}_0 = [0 \quad 0 \quad 0 \quad 0 \quad 0]^T \quad (28)$$

The initial control input and output are similarly defined. Figure 4 is a flowchart describing this initialization and the subsequent simulation method. A loop is then set up to calculate the change in states for each time step. The number of time steps is  $nframes$ , and is determined using the total time the simulation is to be run,  $t_{final}$ , and  $h$ , as shown in Figure 4. As the simulation runs through each loop, the states from the previous loop,  $\mathbf{x}_k$ , or the initial states if it is the first time through, as well as the control input,  $\mathbf{u}_k$ , is used to calculate the change in the states,  $\mathbf{x}_{k+1}$ . This state vector and the control vector are also used to determine the output vector,  $\mathbf{y}_k$ , which is stored after adding in the steady-state values to the states.  $\mathbf{x}_{k+1}$  is then mapped into  $\mathbf{x}_k$  to be used in the next loop. This process continues until the simulation runs through the loop  $nframes$  times. Using the stored output vectors at each time step, the times histories of the states are plotted. The simulation is coded using MATLAB 7.0. By loading values determined from AAA for a given flight condition into a LTI state-space model in MATLAB, the discretized model can be determined using commands imbedded in the program. This is done for both a clean aircraft and an iced aircraft.

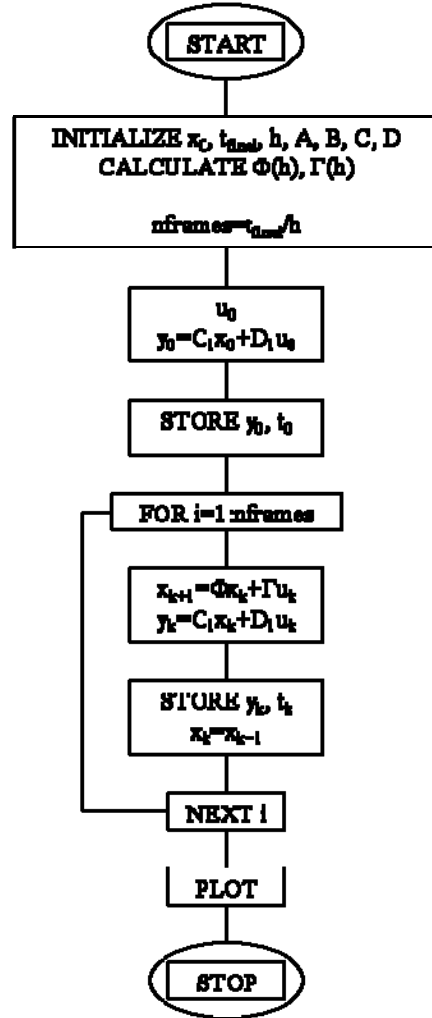


Figure 4. State Transition Method Simulation Flowchart<sup>21</sup>

#### IV. Modeling and Incorporation of Icing Effects

The extent to which each stability and control derivative is affected by ice accretions is based on previous studies, in particular those concerning the flight dynamics of a DeHavilland Twin Otter.<sup>8,19</sup> Twin Otter data was used because there is more icing data available of the type needed for this research than for any other aircraft reported in the open literature. In general, the effectiveness of  $C_{y_{\beta}}$ ,  $C_{y_{\delta_r}}$ ,  $C_{l_{\beta}}$ ,  $C_{l_p}$ ,  $C_{l_{\delta_a}}$ ,  $C_{l_{\delta_r}}$ ,  $C_{n_{\beta}}$ ,  $C_{n_r}$ , and  $C_{n_{\delta_r}}$  have been observed to degrade between 5% and 25%. As ice builds up on the leading edge of the wing, horizontal tail, and vertical tail, the carefully engineered surfaces are compromised. Thus they produce less lift. Also, the ice accretion may develop horns that protrude into the airflow as well as increasing surface roughness leading to an increase in drag. These changes in lift and drag contribute to changes in rolling and yawing moments, especially in the event that ice only accretes on one half of the wing. The exact amount of degradation, whether it is a change in side-force, rolling moment, or yawing moment depends on both the aircraft configuration and the particular derivative in question.

The percentage of degradation for each derivative of an evenly iced aircraft is imbedded within the MATLAB program that dimensionalizes the values calculated by AAA. Each of these

dimensionalized counterparts of the derivatives is multiplied by an icing factor,  $f_{ice}$ , with values between 0.75 and 1.25 depending on what is needed to cause the derivative in question to become less stable. For example, the modification for  $C_{l_p}$  is

$$L_{\beta_{rot}} = \frac{\bar{q}Sb * (1.000 - f_{ice}) * C_{l_p}}{I_{xx}} \quad (29)$$

such that static stability is reduced as  $C_{l_p}$  decreases. In this case a  $f_{ice}$  value of 10.0% is a degradation factor, meaning that  $C_{l_p}$  becomes less stable by 10%, based on data from the DeHavilland Twin Otter.<sup>8</sup> For the numerical examples these degradation factors are assumed to be the worst case scenario for icing on the Cessna 208B. To analyze how the flight dynamics and performance change with ice accretion severity, additional factors are added to the derivatives to represent various levels of severity. For example, the nominal  $f_{ice}$  degradation factor for  $C_{l_p}$  is 10.0%, as stated above. For a totally iced condition, the worst case for the Cessna 208B is  $f_{ice}$  multiplied by 100%. Similarly, if only mild icing is of interest, then  $f_{ice}$  may only be multiplied by 20%, as shown in the following equation

$$L_{\beta_{rot}} = \frac{\bar{q}Sb * (1.000 - 0.20 * f_{ice}) * C_{l_p}}{I_{xx}} \quad (30)$$

This allows for increased versatility in examining possible effects icing has on the flight dynamics and performance of the aircraft in question.

### A. Asymmetric Icing Effects

Predicting the extent and severity of ice accretion prior to encountering icing conditions can be difficult due to its dependence on the configuration of the aircraft and numerous atmospheric conditions: an aircraft may be easily affected by even the smallest amount of ice, or it may be able to stay in flight without any adverse effects with very severe icing. In addition, an aircraft does not necessarily have to accumulate ice evenly between lifting surfaces or between wing halves. Some aircraft tend to have a wing-icing problem only, others a horizontal tail icing problem, and still others do in fact accumulate ice fairly evenly between lifting surfaces. It is assumed here that the icing effects appear as changes in the lift force and drag force of a given lifting surface, such as a wing or a horizontal tail. Before adding the icing effect to the right half of the wing, an analysis is performed to determine the relative distribution of lift and drag between the wing-fuselage and the horizontal tail. If ice is added to only the right half of the wing the method of applying icing factors to derivatives as described above no longer applies. In this case differences in lift and drag between the clean left wing and iced right wing will be used to determine induced rolling and yawing moments due to ice and integrated in to the state-space model described in previous sections.

This analysis is performed using the 15,000 ft day of trim values. Starting with the relation for total airplane lift coefficient and solving for lift coefficient of the horizontal tail,

$$\begin{aligned}
C_L \bar{q} S &= C_{L_{WF}} \bar{q} S + C_{L_H} \bar{q}_H S_H \\
C_{L_H} &= \frac{C_L \bar{q} S - C_{L_{WF}} \bar{q} S}{\bar{q}_H S_H} = \frac{\bar{q}}{\bar{q}_H} \frac{S}{S_H} (C_L - C_{L_{WF}}) \\
&= \frac{1}{\eta} \frac{S}{S_H} (C_L - C_{L_{WF}}) \\
&= \frac{1}{0.945} \left( \frac{279.4}{70.04} \right) (0.377 - 0.359) \\
&= 0.073
\end{aligned} \tag{31}$$

To determine the lift coefficient of the wing-fuselage combination,

$$\begin{aligned}
C_{L_{WF}} &= C_{L_{o_{WF}}} + C_{L_{\alpha_{WF}}} \alpha_W \\
&= C_{L_{o_{WF}}} + C_{L_{\alpha_{WF}}} (\alpha + i_W) \\
&= 0.034 + 4.779(1.285 + 2.62) \frac{1}{57.3} \\
&= 0.034 + 0.3257 \\
&= 0.359
\end{aligned} \tag{32}$$

Finally, the lift distribution between the horizontal tail and wing is determined using the ratio of (31) and (32) to be

$$\begin{aligned}
\frac{C_{L_H}}{C_{L_{WF}}} &= \frac{0.073}{0.359} = 0.203 \\
C_{L_H} &= 0.203 C_{L_{WF}}
\end{aligned} \tag{33}$$

Thus the horizontal tail generates approximately 20% of the lift that the wing-fuselage generates. Although drag data was not available, drag data for a similar aircraft configuration were used to provide a sanity check on the lift ratio above. Using  $C_{D_{0_w}} = 0.37 C_{D_0}$ , and  $C_{D_{0_H}} = 0.07 C_{D_0}$ ,

$$C_{D_{0_H}} = \frac{0.07}{0.34} = 0.21 C_{D_{0_w}} \tag{34}$$

which confirms that the horizontal tail drag is also in the approximate proportion of 20% of the drag of the wing. Based on the values obtained in (33) and (34), a 20% proportion is selected for the asymmetric icing condition.

The next challenge is to calculate the change in lift and drag if ice accumulates on the right half of the wing only and the resulting rolling and yawing moments. The right half of the wing is chosen because the resulting differences in lift and drag between the two wing halves will thus result in positive lateral/directional moments. The component buildup method is used employing the lifting surface asymmetry described above. The percent due to solely to the wing is then halved for the both the lift and drag equations. Icing factors are then applied, and the iced lift or iced drag is then subtracted from the clean lift and drag equations, as seen in Eq. 35:

$$\begin{aligned}\Delta C_{L_{ice}} &= \frac{1}{2}C_{L_{ice}} - \frac{1}{2}C_L \\ \Delta C_{D_{ice}} &= \frac{1}{2}C_D - \frac{1}{2}C_{D_{ice}}\end{aligned}\tag{35}$$

where the “ice” subscript denotes the right wing with ice applied, and the  $\Delta$  indicates the difference between left and right wing halves.

The difference in lift coefficient and drag coefficient are then dimensionalized as angular accelerations by Eq. 36 and Eq. 37:

$$\Delta L_{ice} = \frac{\Delta C_{L_{ice}} \bar{q} S d_{mgc}}{I_{xx}}\tag{36}$$

$$\Delta N_{ice} = \frac{\Delta C_{D_{ice}} \bar{q} S d_{mgc}}{I_{zz}}\tag{37}$$

where  $d_{mgc}$  denotes the distance along the body X-axis from the mean geometric chord to the airplane centerline. These angular accelerations are then integrated into the state-space equations described in previous sections.

## V. Simulation Validation and Verification

This section validates the mathematics and physics of the aircraft model and simulation, and then verifies that it accurately represents the desired aircraft. For the validation, a series of standard maneuvers were performed and examined for correct flight characteristics corresponding to a conventional aircraft configuration with conventional controls. For the verification, flight test data from Ref. 18 was compared to the responses generated by the state-space model at a cruise flight condition.

### A. Validation

The aircraft model was subjected to several validation maneuvers to determine if the aircraft model responds correctly and consistently to control inputs. For brevity, only one maneuver, a level right bank to validate the lateral dynamics, is reproduced here. It consists of a level right bank from trim with the aileron deflection as the only modulating control. This maneuver should result in an increase in roll rate, an increase in yaw rate, and an increase in sideslip angle due to adverse yaw. The level right bank maneuver is performed by holding the rudder at a constant trim deflection and changing the aileron deflection. This simulation starts from a trim aileron deflection of 0.18 degrees and changes from 0.18 degrees to 5.18 degrees over a period of 10 seconds. Results are only plotted up to 20 seconds because the response of the aircraft at the given flight conditions is adequately represented in that amount of time. The flight conditions for the test are shown in Table 1, and the responses in Figure 5.

Table 1 Level Right Bank Validation Maneuver Flight Conditions and Trim Conditions

Altitude (ft)	Airspeed (kts)	Dynamic Pressure (lbs/ft <sup>2</sup> )	Weight (lbs)	c.g. ( $\bar{c}$ )	$\alpha_1$ °	$\beta_1$ °	$\delta_{a1}$ °	$\delta_{r1}$ °
15000.	135.	35.219	8402.	0.289	5.51	0.13	0.18	-0.95

The bank angle or roll attitude response in Figure 5 shows an almost steady increase once aileron deflection starts to shift at five seconds, and the heading angle response increases correspondingly. Roll rate increases as well as sideslip angle and yaw rate due to adverse yaw, as expected. The rudder time history simply shows that it is being held constant while aileron deflection is increased. These results are reasonably accurate with respect to the physics involved, and indicate that the aircraft model responds properly to an aileron input. The other validation maneuvers (not shown) also supported the conclusion of correct validation.

## B. Verification

Four verification maneuvers were performed and compared to flight test data, to ensure that the simulation accurately represents a Cessna 208B Super Cargomaster. Flight test data was available for

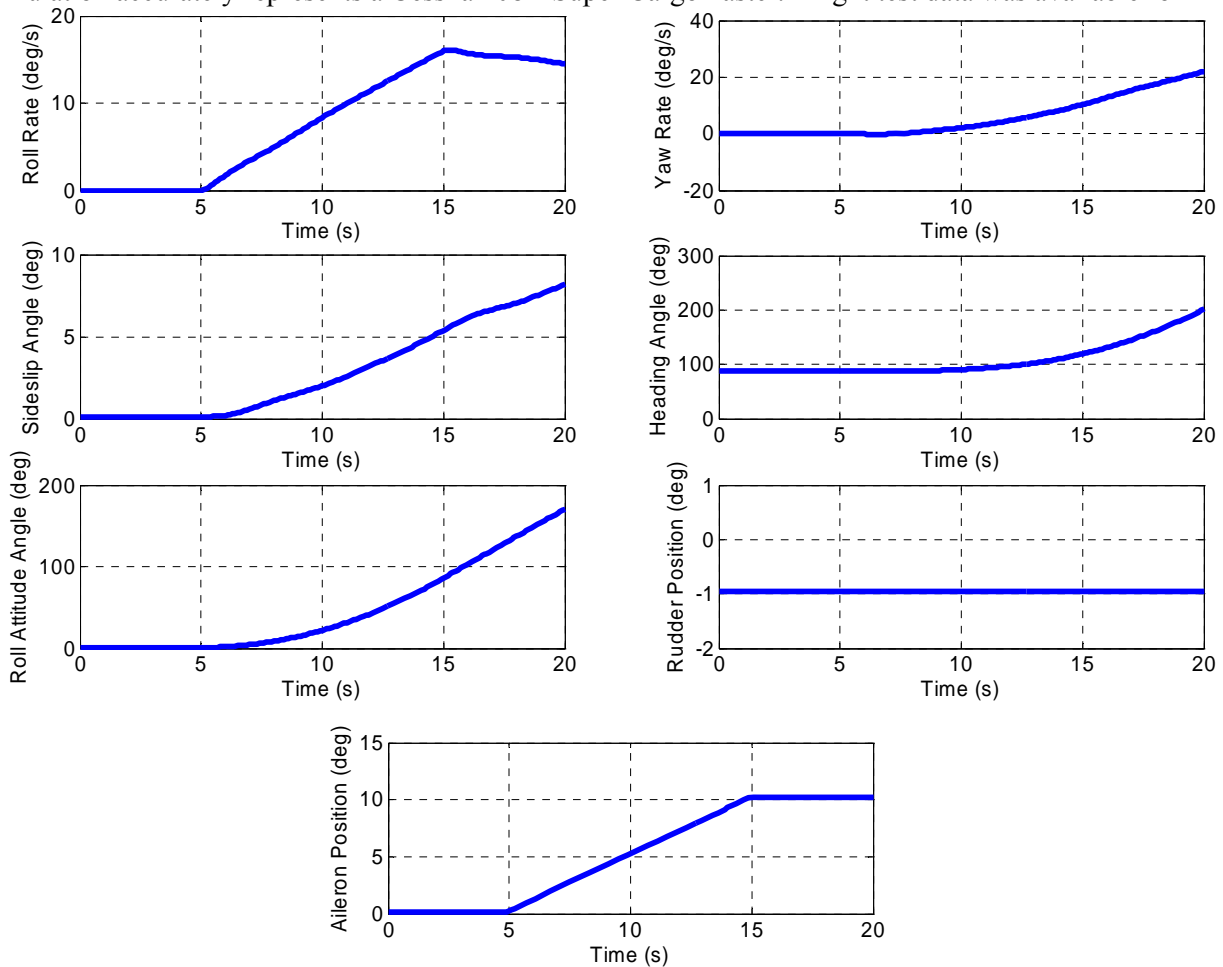


Figure 5. Ramp Aileron Input Responses

only a limited set of maneuvers, from which the verification maneuvers were selected. For brevity, only one lateral/directional maneuver is reproduced here. The maneuver is an aileron singlet, which excites the roll mode and verifies the lateral/directional dynamical model.

### 1. Lateral/Directional Dynamics-Aileron Singlet

Flight and trim conditions for the lateral/directional dynamics verification maneuver are shown in Table 2. The simulation and flight test aircraft are both subjected to an aileron singlet to excite Dutch roll, (and to a lesser extent) roll, and spiral responses. To ensure the greatest accuracy in comparing the simulation to flight test data, the aileron and rudder deflection histories recorded from flight test was used directly as the control inputs for the simulation. The time histories of the states and control surface deflections for both the flight test data and the simulation are shown in Figure 6. Examination of the sideslip angle, roll rate, yaw rate, roll attitude, and heading shows that the simulation responds very closely to the test aircraft. There are minimal errors in each on the order of perhaps 2%.

Table 2 Lateral/Directional Verification Maneuver Flight Conditions and Trim Conditions

Altitude (ft)	Airspeed (kts)	Dynamic Pressure (lbs/ft <sup>2</sup> )	Weight (lbs)	c.g. ( $\bar{c}$ )	$\alpha_1$ °	$\beta_1$ °	$\delta_{a1}$ °	$\delta_{r1}$ °
15000.	135.	40.97	8402.	0.289	1.28	0.13	0.18	-0.95

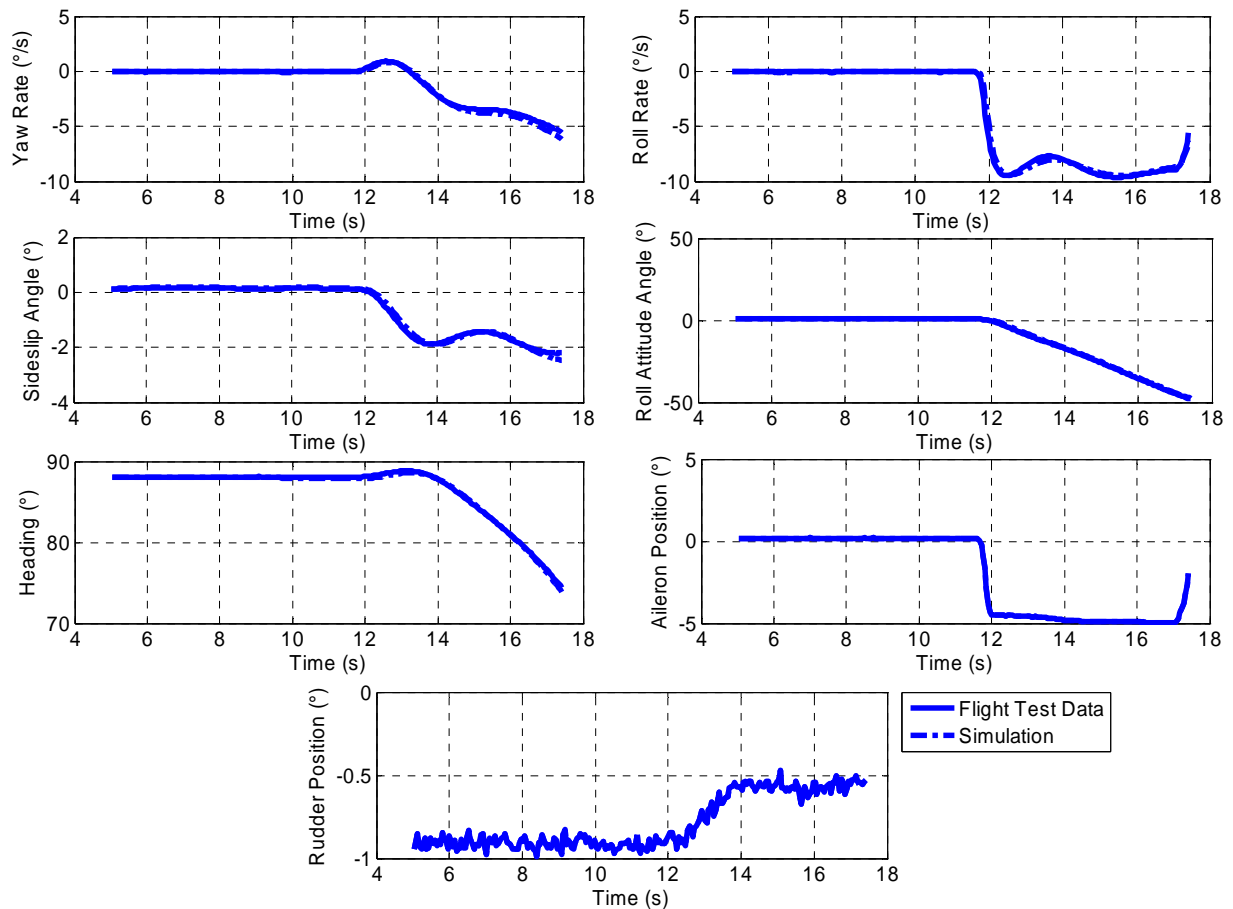


Figure 6. Aileron Singlet Verification Maneuver Responses

Mismatches or errors noted in Figure 6 between the flight test data and the simulation model arise from several sources. The first is that the simulation is a linear time-invariant model of a highly nonlinear time-variant system, so small changes in the engine performance or control surface deflections are not accounted for in the model. Also, the model does not take into account external perturbations such as gusts that probably affected the flight test aircraft to some extent during the test flights. Despite these inaccuracies, the response is generally as expected, and the lateral/directional model is judged to be acceptable as an accurate representation of the aircraft, within the limitations and accuracies of the methods used to construct the model.

## VI. Numerical Examples

The simulation was used to evaluate several lateral/directional control inputs uneven icing scenarios for the purpose of determining the change in both dynamic response and performance due to various levels of ice accretion. One parameter identification type maneuver consisting of a rudder triplet followed closely by an aileron doublet and two cases of ice on the right half of the wing only are presented to demonstrate the prediction of icing effects on aircraft states and parameters such as roll rate, yaw rate, and sideslip angle. The data presented in Table 3 and Table 4 represents mixed icing conditions.<sup>8</sup> These are the degradation factors that are applied to the stability and control derivatives shown in Eq. 29, and they indicate how much the lateral stability decreases for each derivative in the case of evenly accreted ice and the whole aircraft, and how much lift decreases and drag increases for the case of uneven accretion of ice on the right half of the wing. Subtracting each percentage from unity and applying it to the derivative indicated will effectively modify the aircraft model for icing. In addition, an increase of 15% was applied to the total drag, based on data obtained for the Twin Otter that shows an increase in drag of anywhere from 5% to ~30%.<sup>8,19</sup> For the purpose of direct comparison, weight and airspeed are the same for each case, shown in Table 5.

Table 3 Percent Change in Stability and Control Derivatives Due to Icing<sup>8</sup>

derivative	$\Delta C_{Z_0}$	$\Delta C_{Z_\alpha}$	$\Delta C_{Z_q}$	$\Delta C_{Z_{\delta e}}$	$\Delta C_{m_0}$	$\Delta C_{m_\alpha}$	$\Delta C_{m_q}$	$\Delta C_{m_{\delta e}}$
definition	$(-\Delta C_{L_0})$	$\Delta(-C_{L_\alpha}-C_{Dl})$	$(-\Delta C_{L_q})$	$(-\Delta C_{L_{\delta e}})$	$(\Delta C_{m_0})$	$(\Delta C_{m_\alpha})$	$(\Delta C_{m_q})$	$(\Delta C_{m_{\delta e}})$
$f_{ice}$	0	-10.0	-1.352	-9.539	0	-9.924	-3.509	-10.0

Table 4 Percent Change in the Lateral/Directional Stability and Control Derivatives Due to Icing<sup>8</sup>

derivative	$\Delta C_{Y_\beta}$	$\Delta C_{Y_{\delta r}}$	$\Delta C_{l_\beta}$	$\Delta C_{l_p}$	$\Delta C_{l_{\delta a}}$	$\Delta C_{l_{\delta r}}$	$\Delta C_{n_\beta}$	$\Delta C_{n_r}$	$\Delta C_{n_{\delta a}}$
$f_{ice}$	-20.0	-8.0	-10.0	-10.0	-10.0	-8.0	-20.0	-6.111	-8.330

Table 5 Flight and Trim Conditions for Cases 1 – 3

Altitude (ft)	Airspeed (kts)	Dynamic Pressure (lbs/ft <sup>2</sup> )	Weight (lbs)	c.g. ( $\bar{c}$ )	$\alpha_1$ °	$\beta_1$ °	$\delta_{a1}$ °	$\delta_{r1}$ °
15000.	135.	35.219	8402.	0.289	5.51	0.13	0.18	-0.95



yaw rate, respectively, between the configurations. Also supported here are maximum differences in the sideslip angle, heading angle, and roll attitude angle on the order of 10%. However, despite these differences the iced aircraft returns trim, which suggests that it is still inherently stable.

### **B. Case 2: Uneven Asymmetric Icing, 20% Iced Configuration**

This Case represents an aircraft with “mild” ice accretions on only one half of the wing. The ice accretions are known to alter the shape of the carefully engineered airfoil, thus decreasing its effectiveness at generating lift as well as increasing drag. Studies conducted at the University of Illinois on various airfoils with different types of ice accretions support this observation.<sup>20</sup> As a result of this uneven icing and the resulting differences in lift and drag between the iced half and non-iced half of the wing, an ice induced rolling moment and yawing moment develop. This maneuver simply consists of allowing the aircraft to respond to these lateral/directional moments and noting the roll-off tendencies of the iced aircraft without any control inputs. This open-loop simulation does not have a human pilot to correct for these induced moments and in known icing conditions the autopilot would not be used.

Figure 8 shows, as expected, that without any disturbances the clean aircraft remains at trim. The iced aircraft, however, begins to respond to the induced moments almost immediately. Both the roll rate and yaw rate time histories show that the aircraft has become unstable and quickly diverges. After only five seconds, the roll rate has already increased to 125 deg/sec whereas the yaw rate increases to 42 deg/sec. Since the ice is applied to the right wing, the induced moments consist of a positive rolling moment as well as a positive yawing moment. This is seen in Figure 8 in the sideslip angle, heading angle, and roll attitude angle time histories. The positive rolling moment due to ice results in the roll attitude angle increasing to 125 degrees within 5 seconds. The iced aircraft has practically flipped over. The positive yawing moment due to ice causes the sideslip angle to increase to -20 degrees within 5 seconds and the resulting heading angle to increase to 130 degrees. This is effectively summarized by noting that the time-to-double is 0.67 sec. Many aircraft of this class cannot handle extreme sideslip angles or the swift inversion, so even with mild icing this imbalance in ice distribution quickly leads to full departure from controlled flight of the aircraft.

### **C. Case 3: Uneven Asymmetric Icing, Fully Iced Configuration**

This Case represents a “worst-case” scenario: aircraft with one half of the wing fully accreted by ice. The full factors listed in Table 3 are applied to the model. This maneuver also consists of allowing the aircraft to respond to the ice induced lateral/directional moments and noting the roll-off tendencies of the iced aircraft.

Figure 9 shows that the time histories for this “fully developed” ice accretion case are dynamically similar in character to those of Case 2, but the differences between the clean configuration and the fully iced configuration are much more pronounced here in Case 3. The aircraft has still become unstable as shown in Figure 9 as all of the states diverge. Roll rate and yaw rate have increased 600 and 210 deg/sec, respectively. Sideslip angle has increases to an extreme value of -100 degrees in only 5 seconds. Consistent with these results are a roll attitude angle of over 650 degrees and a heading angle of 300 degrees. These results indicate that within five seconds and given no compensatory control inputs, the iced aircraft is spinning about both the roll axis and yaw axis. These results can also be effectively summarized by the time-to-double. For this case the time-to-double is 0.25 sec, which also results in full departure from controlled flight of the aircraft.

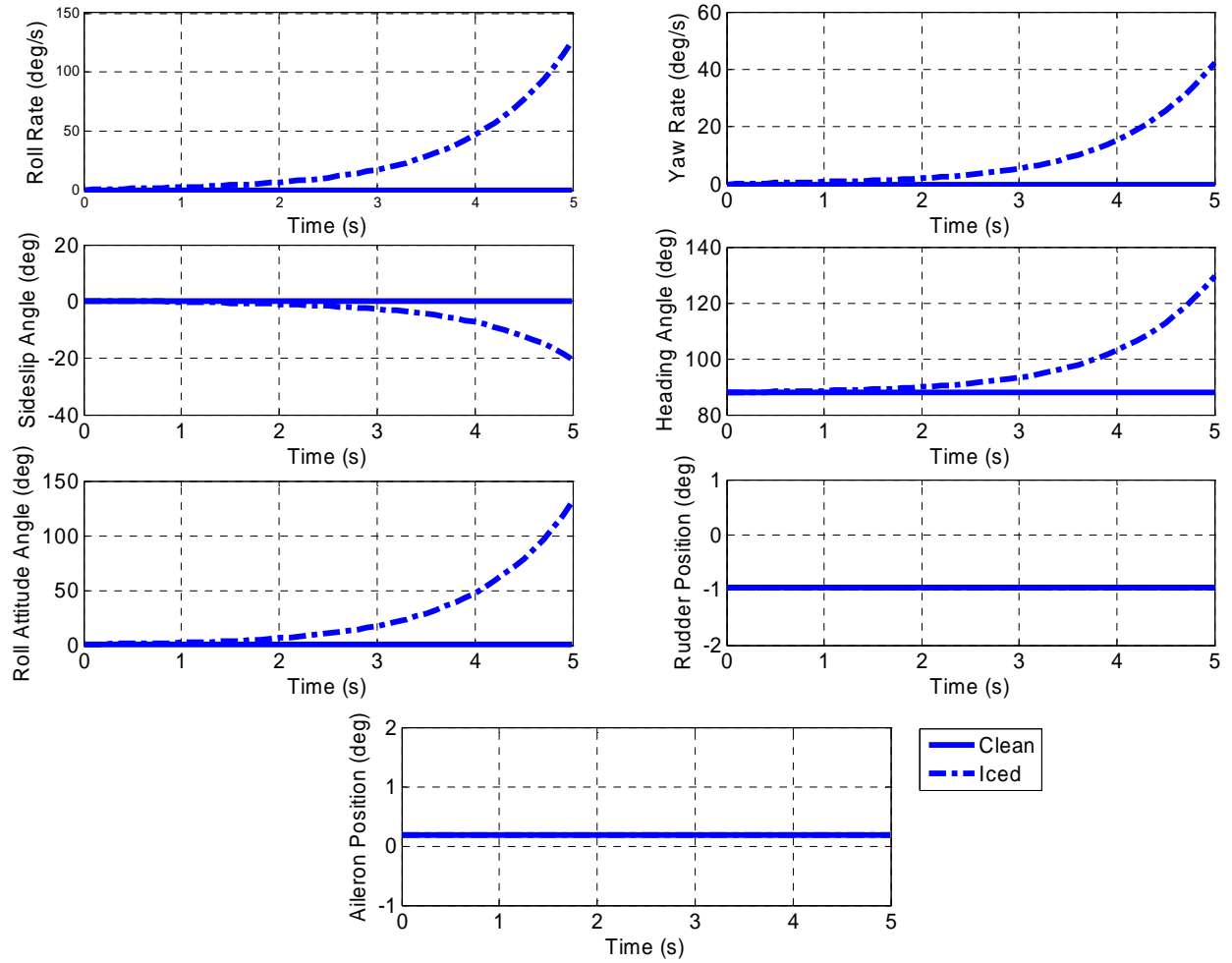


Figure 8. Case 2 Time Histories of Clean Aircraft and Aircraft with Right Wing Half 20% Iced

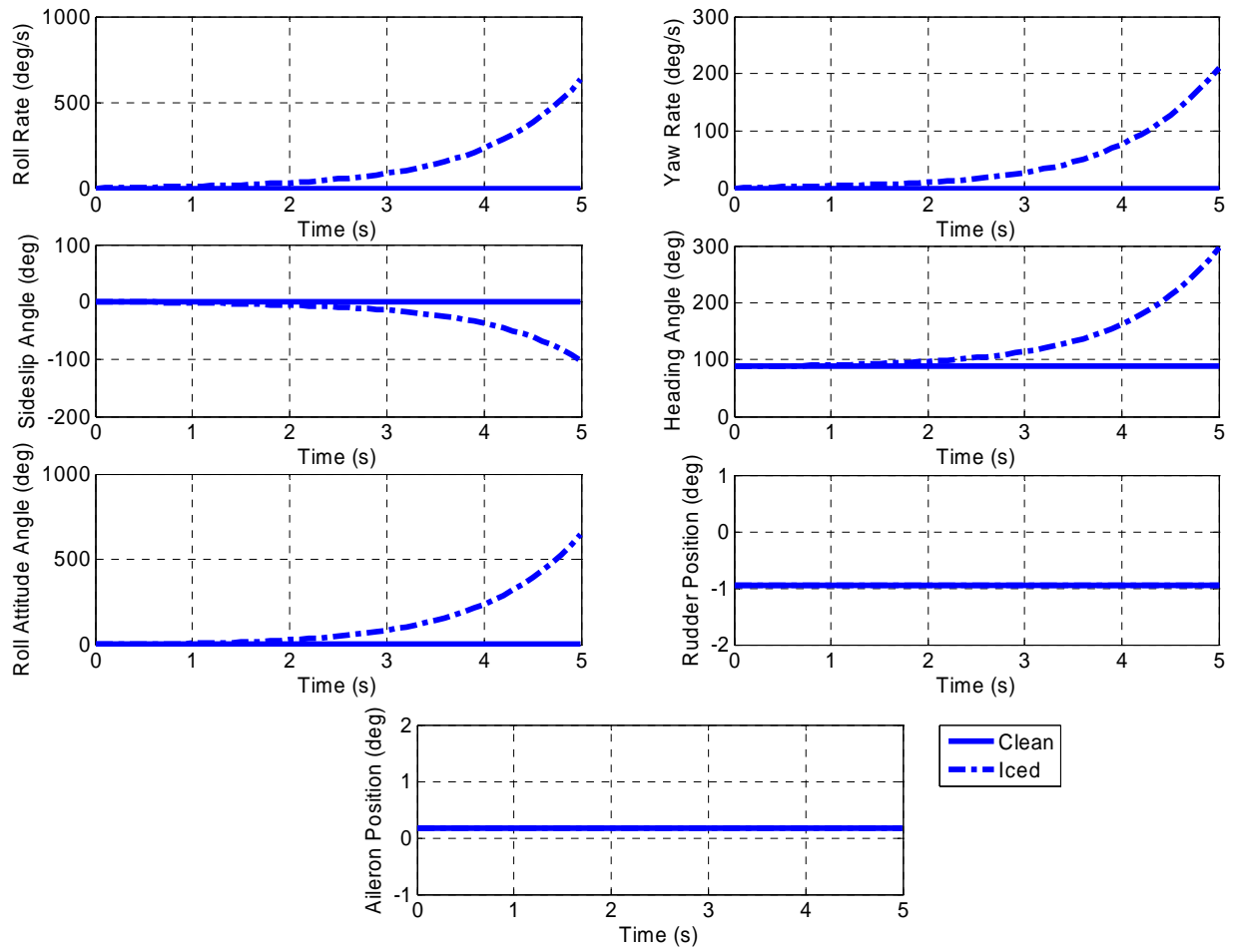


Figure 9. Case 3 Time Histories of Clean Aircraft and Aircraft with Right Wing Half Fully Iced

## VII. Conclusions and Recommendations for Further Research

An analysis method using flight data, wind tunnel data, and the United States Air Force Data Compendium was developed to create a basic but reasonably detailed and accurate simulation model that accounts for the effects of ice accretion on light aircraft. The component build-up method was used to implement icing effects one half of the wing alone and combined wing and horizontal tail using icing data on similar light aircraft. The icing data used was obtained empirically, and modified for the aircraft configuration considered. The scope of the present work was limited to the lateral/directional axis, where the some detrimental icing effects are experienced. A linear time invariant, state-space model of the lateral/directional model of a representative light aircraft was developed, and used for non real-time simulation to evaluate icing effects on stability and control characteristics, in addition to effects on roll-off tendencies. Validation of the simulation model was conducted using several basic maneuvers, and verification was conducted using flight test data for the same aircraft as the simulation. Numerical examples consisting of a parameter identification type maneuver and two uneven icing roll-off assessments in various levels of icing were evaluated, and based on the results presented in the paper the following conclusions are drawn:

1. The linear state-space model representation, discrete simulation model, and inclusion of simplified icing effects appear to be an adequate tool for basic icing dynamics and performance analysis for the maneuvers investigated. Verification results to flight data showed good agreement for the maneuvers investigated here, and only relatively simple data was needed to construct the models.
2. Qualitatively, from the simulation results evenly distributed ice caused the aircraft to become less stable, but the evenly iced aircraft remains inherently stable for the type of maneuver investigated.
3. For the uneven accretion comparisons of iced aircraft to clean aircraft allowing the iced aircraft to respond to ice induced moments without any control inputs, simulation results showed an adverse affect on lateral/directional stability:
  - a. The 20% iced right wing half configuration experienced the following within 5 seconds:
    - i. First-order departure from controlled flight
    - ii. Time-to-double=0.67 sec
  - b. The 100% iced right wing half configuration experienced the following within 5 seconds:
    - i. First-order departure from controlled flight
    - ii. Time-to-double=0.25 sec

Future work will improve the fidelity of the simulation. A vortex lattice method code will be used to attempt to model the classic horn shaped leading edge ice shape, including surface roughness effects, for the purpose of extracting stability derivative increments to incorporate into the simulation. A complete ensemble of test cases corresponding to a wide variety of altitudes will be run and compared to the maneuvers presented in this paper. A control input scheme to attempt to compensate for the uneven icing between wing halves will be developed. Finally, the severity of the ice accretions will be varied within the simulation to compare the differences in degradation from one case to another.

## VIII. Acknowledgment

This research is funded by the Aeronautical and Educational Services Company, under grant number C05-00356. The technical monitor is Dr. Donald T. Ward. The authors gratefully acknowledge this support.

## IX. References

- <sup>1</sup> Anonymous, "Annual Review of Aircraft Accident Data: U.S. General Aviation, Calendar Year 1998". National Transportation Safety Board. Washington, DC. 2003. p. 35, 39.
- <sup>2</sup> Anonymous, "Annual Review of Aircraft Accident Data: U.S. General Aviation, Calendar Year 1999". National Transportation Safety Board. Washington, DC. 2003. p. 32, 39.
- <sup>3</sup> Anonymous, "Annual Review of Aircraft Accident Data: U.S. General Aviation, Calendar Year 2000". National Transportation Safety Board. Washington, DC. 2004. p. 38, 41.
- <sup>4</sup> Anonymous, "Annual Review of Aircraft Accident Data: U.S. General Aviation, Calendar Year 1997". National Transportation Safety Board. Washington, DC. p. 38, 41.
- <sup>5</sup> Gurbacki, H.M. and Bragg, M.B.. "Unsteady Aerodynamic Measurements on an Iced Airfoil". AIAA Paper 2002-0241. Reno, NV. 2002.
- <sup>6</sup> Bragg, M.B.. "Aircraft Aerodynamic Effects Due To Large Droplet Ice Accretions". AIAA Paper 96-0932. Reno, NV. 1996.
- <sup>7</sup> Ratvasky, T.P. and Ranaudo, T.J., "Icing Effects on Aircraft Stability and Control Determined from Flight Data," NASA TM 105977 and AIAA Paper 93-0398. Jan. 1993.
- <sup>8</sup> Bragg, M.B., Hutchison, T., Merret, J., Oltman, R., and Pokhariyal, D.. "Effect of Ice Accretion on Aircraft Flight Dynamics". AIAA Paper 2000-0360. Reno, NV. 2000.
- <sup>9</sup> Rauw, Marc, "FDC 1.3 – A SIMULINK Toolbox for Flight Dynamics and Control Analysis," 1998, available at <http://www.mathworks.com/matlabcentral/fileexchange>.
- <sup>10</sup> Sharma, V., Voulgaris, P.G., and Frazzoli, E., "Aircraft Autopilot Analysis and Envelope Protection for Operation Under Icing Conditions," *Journal of Guidance, Control, and Dynamics*, Vol. 27, No. 3, pp. 454-465, 2004.
- <sup>11</sup> Sibilski, K., Lasek, M., Ladyzynska-Kozdras, E., and Maryniak, J., "Aircraft Climbing Flight Dynamics With Simulated Ice Accretion," AIAA Paper 2004-4948, Providence, RI, Aug. 2004.
- <sup>12</sup> Lee, S. and Bragg, M.B., "Experimental Investigation of Simulated Large-Droplet Ice Shapes on Airfoil Aerodynamics," *Journal of Aircraft*, Vol. 36, No. 5, 1999, pp. 844-850.
- <sup>13</sup> Broeren, A.P., Addy, Jr., H.E., and Bragg, M.B., "Effect of Intercycle Ice Accretions on Airfoil Performance," *Journal of Aircraft*, Vol. 41, No. 1, 2004, pp. 165-174; also AIAA Paper 2002-0240, Jan. 2002.
- <sup>14</sup> Whalen, E., and Bragg, M., "Aircraft Characterization in Icing Using Flight-Test Data," *Journal of Aircraft*, Vol. 42, No. 3, 2005, pp. 792-794.
- <sup>15</sup> Broeren, A.P. and Bragg, M.B., "Effect of Airfoil Geometry on Performance with Simulated Intercycle Ice Accretions," *Journal of Aircraft*, Vol. 42, No. 1, 2005, pp. 121-130; also AIAA Paper 2003-0728, Jan. 2003.
- <sup>16</sup> Advance Aircraft Analysis, Design, Analysis, and Research Corporation, Lawrence, KS, 2003.

- <sup>17</sup> Anonymous, Cessna Aircraft Company Model 208 Maintenance Manual
- <sup>18</sup> Kohlman Systems Research, Lawrence, KS.
- <sup>19</sup> Bragg, M.B. and Lee, S. “Aircraft Icing Flight Dynamics Model for Twin Otter Aircraft”. Urbana, IL. 2000.
- <sup>20</sup> Jackson, D.G. and Bragg, M.B.. “Aerodynamic Performance of an NLF Airfoil with Simulated Ice”. AIAA Paper 99-0373. Reno, NV. 1999.
- <sup>21</sup> Valasek, J., Aero 625 course notes, aerospace engineering department, Texas A&M University, 1998.
- <sup>22</sup> B. De Schutter, “Minimal state-space realization in linear system theory: An overview,” Journal of Computational and Applied Mathematics, Special Issue on Numerical Analysis in the 20th Century – Vol. I: Approximation Theory, vol. 121, no. 1-2, p. 331-354, Sept. 2000.
- <sup>23</sup> Bragg, M.B., Perkins, W.R., Sarter, N.B., Basar, T., Voulgaris, P.G., Gurbacki, H.M., Melody, J.W., and McCray, S.A.. “An Interdisciplinary Approach to Inflight Aircraft Icing Safety”. AIAA Paper 98-0095. Reno, NV. 1998.
- <sup>24</sup> Anonymous, National Transportation Safety Board Final Report: DEN03FA012.
- <sup>25</sup> Lee, S. and Bragg, M.B.. “Effects of Simulated-Spanwise-Ice Shapes on Airfoils: Experimental Investigation”. AIAA Paper 99-0092. Reno, NV. 1999.
- <sup>26</sup> Bragg, M.B., Basar, T., Perkins, W.R., Selig, M.S., Voulgaris, P.G., Melody, J.W., and Sarter, N.B.. “Smart Icing Systems for Aircraft Icing Safety”. AIAA Paper 2002-0813. Reno, NV. 2002.
- <sup>27</sup> Hossain, K.N., Sharma, V., Bragg, M.B., and Voulgaris, P.G.. “Envelope Protection and Control Adaptation in Icing Encounters”. AIAA Paper 2003-0025. Reno, NV. 2003.
- <sup>28</sup> Lu, B. and Bragg, M.B.. “Airfoil Drag Measurement with Simulated Leading-Edge Ice Using the Wake Survey Method”. AIAA Paper 2003-1094. Reno, NV. 2003.
- <sup>29</sup> Pan, J., Loth, E., and Bragg, M.B.. “RANS Simulations of Airfoils with Ice Shapes”. AIAA Paper 2003-0729. Reno, NV. 2003.
- <sup>30</sup> Broeren, A.P., Addy, Jr., H.E., and Bragg, M.B.. “Flowfield Measurements About an Airfoil with Leading-Edge Ice Shapes”. AIAA Paper 2004-0559. Reno, NV. 2004.

## Appendix: Linear State-Space Models of Cessna 208 Super Cargomaster

Lateral/Directional dynamics (all angular quantities in radians):

Flight Condition: 135 kts, 15000 ft, 35.291 lbs/ft<sup>2</sup>

$$\begin{bmatrix} \dot{p} \\ \dot{\phi} \\ \dot{\beta} \\ \dot{r} \\ \dot{\psi} \end{bmatrix} = \begin{bmatrix} -4.10 & 0 & -5.96 & 0.77 & 0 \\ 1 & 0 & 0 & 0.10 & 0 \\ -0.0014 & 0.14 & -0.17 & -0.99 & 0 \\ -0.19 & 0 & 2.16 & -0.52 & 0 \\ 0 & 0 & 0 & 1.00 & 0 \end{bmatrix} \begin{bmatrix} p \\ \phi \\ \beta \\ r \\ \psi \end{bmatrix} + \begin{bmatrix} 8.99 & 1.10 \\ 0 & 0 \\ 0 & 0.04 \\ -0.07 & -2.63 \\ 0 & 0 \end{bmatrix} \begin{bmatrix} \delta_A \\ \delta_R \end{bmatrix}$$

Flight Condition: 135 kts, 15000 ft, 35.291 lbs/ft<sup>2</sup>

$$\begin{bmatrix} \dot{p} \\ \dot{\phi} \\ \dot{\beta} \\ \dot{r} \\ \dot{\psi} \end{bmatrix} = \begin{bmatrix} -4.77 & 0 & -6.93 & 0.90 & 0 \\ 1 & 0 & 0 & 0.02 & 0 \\ -0.0018 & 0.14 & -0.22 & -0.99 & 0 \\ -0.22 & 0 & 2.51 & -0.61 & 0 \\ 0 & 0 & 0 & 1.00 & 0 \end{bmatrix} \begin{bmatrix} p \\ \phi \\ \beta \\ r \\ \psi \end{bmatrix} + \begin{bmatrix} 10.46 & 1.28 \\ 0 & 0 \\ 0 & 0.05 \\ -0.08 & -3.06 \\ 0 & 0 \end{bmatrix} \begin{bmatrix} \delta_A \\ \delta_R \end{bmatrix}$$